LES of cross flow induced vibrations in square normal cylinder array

Vilas Shinde, Elisabeth Longatte-Lacazedieu, Franck Baj

LES of cross flow induced vibrations in square normal cylinder array

Vilas Shinde[1], **Elisabeth Longatte, Franck Baj**

IMSIA, EDF-CNRS-CEA-ENSTA UMR 9219, Clamart Cedex, France

Abstract

Large eddy simulations (LES) of a single phase water flow through square normal tube bundle at Reynolds numbers from 2000 *to* 6000 *is performed to investigate the fluid-elastic instability. A single cylinder is allowed to oscillate in one degree of freedom (1-DOF) in flow normal direction, similar as in experiments. The fluid-structure coupling is simulated using the Arbitrary Lagrangian-Eulerian (ALE) apporach. The sub-grid scale turbulence is modeled using standard Smagorinsky's eddy-viscosity model. The LES results show good agreement with experimental results in terms of the response frequency and damping ratio of the cylinder. The dynamic case simulations are compared with static cases over the range of Reynolds numbers by means of the probe velocity spectra and pressure profiles on the cylinder surface.*

Mots clefs : Large Eddy Simulation, Flow Induced Vibration, Tube Arrays

1 Introduction

Heat exchangers are vital component of any power industry. Fluid flow through tube bundles induce vibrations and may result in severe breakdown. The cross flow induced vibrations in tube arrays are classified mainly in four categories, namely: turbulent buffeting, vibrations due to flow periodicity (or vortex induced vibrations), acoustic vibrations and fluid-elastic instability. The fluid-elastic instability is most devastating compared to all, yet less understood. Large amount of research work is performed on this phenomenon to enhance understanding of the stability limit criteria, in order to prevent its occurrence. Many theoretical models has been developed since the phenomenon was first brought to notice by Roberts [4] and later by Connors [7]. The models proposed for the phenomenon include Blevins [5], Tanaka et al. [9], Chen et al. [19,20], Paidoussis and Price [13], Lever and Weaver [10], Granger et. al [8] etc.. Thus providing an insight into fluid-elastic instability by means of different instability mechanisms

[1]Corresponding author: vilas.j.shinde@gmail.com

such as 'fluid flow jet switching mechanism', 'stiffness controlled mechanism', 'damping controlled mechanism' etc.. In addition, dynamic features of the instability such as phase lag between fluid force and displacement, flow cell with boundary layer effect are considered while modeling the phenomenon. Although many approaches exist, all fall short individually to predict the phenomenon for wide range of parameters.

In addition to the experiments, Computational Fluid Dynamics (CFD) provides a possibility to simulate and better understand such phenomena. In the industrial context, Direct Numerical Simulation (DNS) is computationally expensive. Large Eddy Simulation (LES) overcomes the shortcoming of URANS approach by capturing the transient features of the flow physics. Contrary to the DNS approach, LES provide a feasibility to simulation such problems by modeling the sub-grid-scale turbulence. Some of the early works on simulation of flow through tube bundles using LES include the work of Hassan and Barsamian (1997, 1999). Further, the work of Rollet-Miet et al [15], Benhamadouche and Laurence [17] and C. Liang and G. Papadakis [6] confirmed the benefits of LES over URANS for tube bundle geometries. Although Large Eddy Simulation (LES) is still not reachable for high Reynolds number as it requires high computational resources, it is suitable for low Reynolds number. Recently, similar benefits of LES were reported for vortex-induced vibrations at moderate Reynolds number in Jus et. al. [11].

In present work, LES is carried out to simulate single-phase fluid, cross flow induced vibration in square normal cylinder arrangement, for several gap Reynolds numbers from 2000 to 6000, in order to improve the understanding of fluid-elastic instability. The length of computational domain in spanwise direction is taken as $4D$, which provides enough space for LES vortex dynamics. In many experiments, it has been observed that the fluid-elastic vibrations are pre-dominant in the flow normal direction, especially in water-flow experiments (Price et al. [18]). Also there are several studies performed on a single cylinder oscillating in a fixed cylinders arrangement (Price et al. [18], Khalifa et al. [1]). It leads to essentially the same critical velocities as for the fully flexible array of cylinders. Therefore the central cylinder is only monitored and allowed to oscillated in flow normal direction. Although, in some studies such as Kevlahan [14], the instability is found to be dominant in in-flow direction for wide range of mass-damping parameter and the critical velocities predicted using a single cylinder in fixed array are overestimated compared to the fully flexible array.

2 Configuration

In experiments, the tube bundle (5×5) is located in a vertical flow channel. The cylinders are in square normal arrangement. The two side columns are half wall mounted. Only the cylinder at center is flexibly mounted, while the remaining cylinders are fixed. The channel depth (the length of cylinders) and width are $100 \times 10^{-3}\ m$ and 70×10^{-3} m respectively. The central cylinder is supported on a flexible blade at one end. It is al-

lowed to move in flow normal direction only. The flexible supporting blade is connected to a strain gauge in order to measure the displacement of cylinder.

The tube diameter is $D = 12.15 \times 10^{-3}\ m$. The pitch ratio ($p = P/D$) of the tube arrangement is $p = 1.44$ in both (in-flow and flow normal) directions. The modal mass of the cylinder per unit length is $m = 0.298\ kg/m$. The natural frequency (f_n) and damping ratio (ζ) of the cylinder in air are $14.39\ Hz$ and 0.25% respectively.

The computational domain for LES is $70 \times 10^{-3}\ m$ wide and $48.6 \times 10^{-3}\ m$ deep. The cylinders length is thus $4D$ against about $8D$ in the experimental facility. The domain is $269.5 \times 10^{-3}\ m$ long in in-flow direction. The inflow boundary is $5D$ upstream the tube bundle, while as the outflow is $10D$ downstream of the tube bundle. The tube diameter (D), array pitch ratio (p) and arrangement of the tube bundle (90^o) is identical to the experiment. The geometry of the LES computational domain is shown in Figure 1(a).

The computational domain is descretized in nearly 25.3 million finite volume cells. The mesh near the cylinder surface region is fine enough to resolve the boundary layers of the fluid flow. The first layer of the mesh is placed at a distance of $1.8 \times 10^{-5}\ m$ away from the cylinder surface ensuring the y^+ below 1. The circumference of each cylinder is split in 360 elements. The mesh is coarser ($2 \times 10^{-3}\ m$) far upstream and downstream the tube array. Figure 1 (b) shows the details of mesh inside tube array.

In the Large Eddy Simulation (LES) approach of turbulence modeling, the large eddies (bigger than the size of mesh cells) are resolved directly. It contains most of the turbulent energy, however the sub-grid scale turbulence need to be modeled in order to balance the truncated turbulence energy spectrum. The unfiltered eddies are assumed to be isotropic and they can be modeled by simple Boussinesq type eddy viscosity relations. There exist several models for the sub-grid scale turbulence. The standard Smagarinsky model is considered in this work with appropriate value of the constant. However, the choice of sub-grid scale model has little influence on the results (rollet1999and, benhamadouche2003coarse) of interest.

The filtered Navier-Stokes equations in incompressible form can be written as,

$$\frac{\partial \tilde{u}_i}{\partial x_i} = 0 \tag{1}$$

$$\frac{\partial \tilde{u}_i}{\partial t} + \tilde{u}_j \frac{\partial \tilde{u}_i}{\partial x_j} = -\frac{1}{\rho}\frac{\partial \tilde{p}}{\partial x_i} + \frac{\partial}{\partial x_j}\left[(\nu + \nu_t)\left(\frac{\partial \tilde{u}_i}{\partial x_j} + \frac{\partial \tilde{u}_j}{\partial x_i}\right)\right] \tag{2}$$

Where $\tilde{u_i}$ is the filtered instantaneous velocity in i direction. The space and time are represented by x_i and t respectively. ρ is the fluid density, while ν, ν_t are the fluid kinematic viscosity and turbulent viscosity respectively. $\tilde{p}$ is the filtered pressure. The subg-grid scale stress tensor is given by Equation (3).

$$\tau_{ij} = -2\nu_t \tilde{S}_{ij} + \frac{1}{3}\tau_{kk}\delta_{ij} \tag{3}$$

The trace term of the sub-grid scale stress tensor is grouped with the pressure ($\tilde{p}$). The

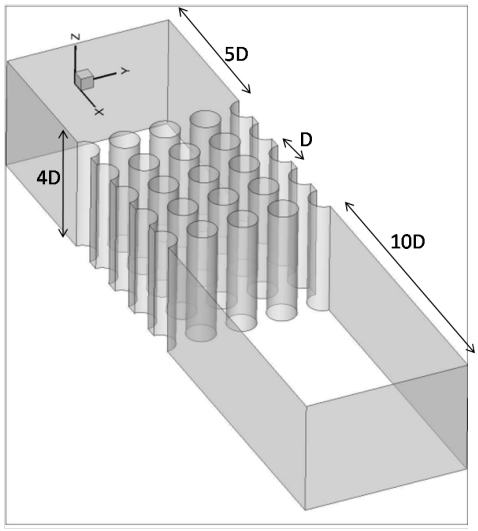

(a) Geometry

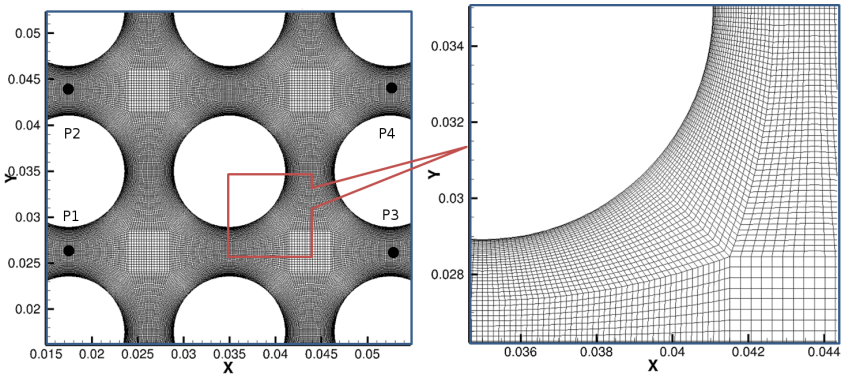

(b) Mesh

Figure 1: Computational Domain with probes ($P1$, $P2$, $P3$ and $P4$)

value for the turbulent viscosity ν_t is provided by Smagorinsky's model (Equation 4).

$$\nu_t = (C_s l_g)^2 \sqrt{2\tilde{S}_{ij}\tilde{S}_{ij}} \tag{4}$$

Where, l_g, C_s are the grid size and Smagorinsky's constant respectively. $\tilde{S}_{ij}$ represents the strain rate tensor. The value of constant C_s is about 0.18 for isotropic turbulence at high Reynolds number. It decrease near wall or in shear flows to about 0.1.

The computations are performed by using $Code\_saturne$, an open-source incompressible Navier-Stokes solver developed by Électricité de France (EDF). It is based on a co-located finite volume method. The second order central difference and Crank-

Nicolson schemes are used to perform the space and time descretizations respectively. A time step has a predictor and a correction steps. In the predictor step all physical properties are calculated along with the velocity field, while as in the correction step the pressure equation is accounted implicitly.

The cylinder movement is coupled with the fluid flow by the method of Arbitrary-Lagrangian-Eulerian (ALE). The moving mesh (boundary) is considered in flow equations in terms of the mesh velocity. In response, the forces experted by the fluid flow are used to displace the cylinder boundary surface. In the experiment, the cylinder is rigid and flexibly mounted. An equivalent numerical arrangement is a mass on spring physics, where, m is the mass of cylinder, k and c are the stiffness and damping coefficients of the cylinder oscillations. The equation of motion for the cylinder can be given by,

$$m\frac{d^2y}{dt^2} + c\frac{dy}{dt} + ky = F_y \tag{5}$$

Where, y is the displacement of the cylinder in flow normal direction, while as the fluid force in the same direction is represented by F_y on the right hand side of equation. The experimental values of modal mass and damping ratio can be used to estimate the stiffness and damping coefficients in air, by using following relations

$$k = (2\pi f_n)^2 m \qquad \text{and} \qquad c = 2\zeta\sqrt{km}$$

The ordinary differential equation (Equation (5)) is numerically solved using Newmark HHT algorithm, in which the fluid forces are used to estimate the displacement y. The new position of the cylinder is achieved by solving Poisson's equation for remeshing before the next flow iteration. The deformation of near-wall mesh is controlled by assigning a high value for an artificial mesh viscosity.

3 Results Analysis

3.1 Comparison

The experiments are performed for Reynolds number Re_g ranging from 2000 up to 6000. The Reynolds number is defined using intertube (gap) velocity u_g m/s and cylinder diameter D m as $Re_g = (\rho u_g D)/(\mu)$, where ρ and μ are fluid density and dynamic viscosity respectively. The non-dimensional reduced velocity is defines as $u^* = (u_g)/(f_n D)$, where f_n is the cylinder response frequency in water at a particular flow velocity (u_g). Figure 2(a) shows the change in response frequency as result of increasing intertube flow velocity. The experimental plot (shown in red color) and the LES simulation plot (shown in green color) show a decreasing trend at the beginning for reduced velocity upto $u^* \approx 1.8$. The response frequency (f_n) curves (Figure 2(a)) show increasing tread from $u^* \approx 1.8$ upto $u^* \approx 2.10$, which is followed by decreased values onset of the instability at about $u^* \approx 3.19$.

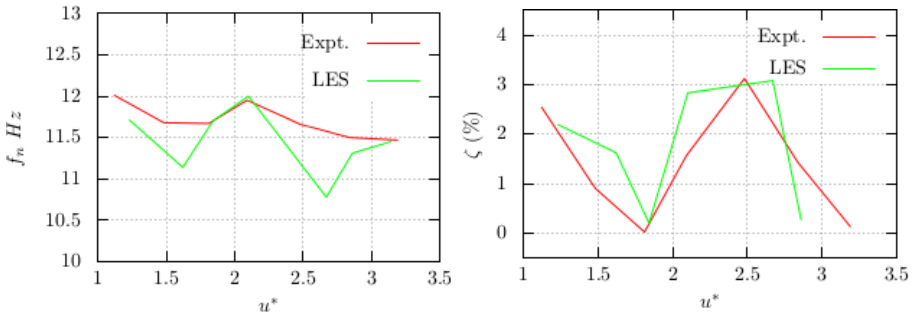

(a) f_n versus u^* (b) ζ versus u^*

Figure 2: Comparison of the cylinder response frequency f_n and damping ratio ζ

The Time Domain Modal Analysis (TDMA) of Poly Reference (PR) type is used to identify the modes and corresponding damping ratios for experimental results, while as the Half Power Bandwith method is suited for LES time response signals. The damping of the cylinder vibrations initially decreases with increase in the gap velocity up to $u_g \approx 0.25\ m/s$ ($u^* \approx 1.8$) (see Figure 2(b)). It is followed by increased values of the damping ratio for reduced velocities $u^* \approx 1.8$ up to $u^* \approx 2.5$. The damping ratio, then follows a monotonous decrease until reaches zero, onset of the instability, in both the experiments and LES results. The critical reduced velocity predicted by LES computations is $u_c^* \approx 3.14$, against an experimental value of $u_c^* \approx 3.19$.

3.2 Analysis

In order to understand the development of fluid-elastic instability, a comparison is done between static case Large Eddy Simulations (LES) results with the dynamic case LES computations. The spectra of Y velocity (u_2) at probe locations $P1$ and $P3$ are compared between static and dynamic cases for increasing reduced velocity (u^*). Further, the velocity spectra at these upstream and downstream locations are compared with the spectrum of cylinder vibration (y) in Figure (3). The natural frequency of the cylinder in the water flow is about $\sim 11.5\ Hz$. In static case, the red curves in Figures 3(a) and 3(b), the shear layer frequency at gap velocity $u_g = 0.175\ m/s$ is 6.5 Hz. In addition, there are harmonics of this frequency in spectra computed at downstream location $P3$. In dynamic case, the green curves in Figures 3(a) and 3(b), there appears an extra frequency peak at both the upstream and downstream locations. It corresponds to the response frequency of cylinder. On other hand, the response spectrum of cylinder, the blue curve in Figures 3(a) and 3(b)) shows a frequency peak at 6.5 Hz. Figures 3(c) and 3(d) show similar comparison for intertube velocity $u_g = 0.262$ m/s. The red curves of static case simulation show two frequency peaks, one at 9.2 Hz and another its harmonic at $\sim 19\ Hz$, at both $P1$ and $P2$ locations. On the contrary, the velocity spectra in dynamic case (green curves in Figures 3(c) and 3(d)) show

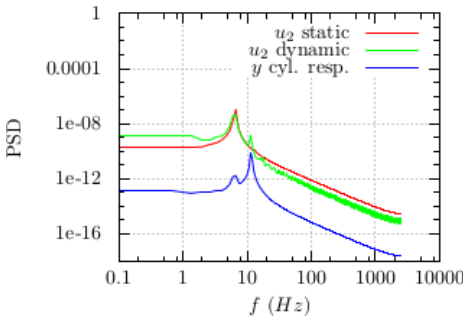

(a) Location $P1$, $u_g = 0.175\ (m/s)$

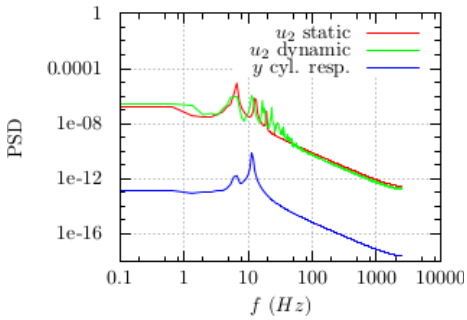

(b) Location $P3$, $u_g = 0.175\ (m/s)$

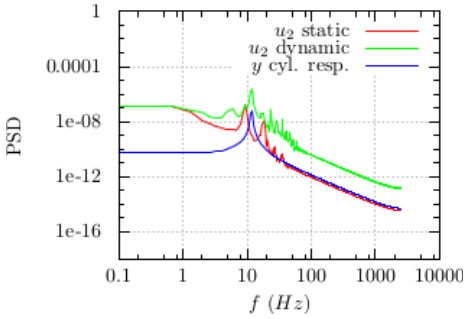

(c) Location $P1$, $u_g = 0.262\ (m/s)$

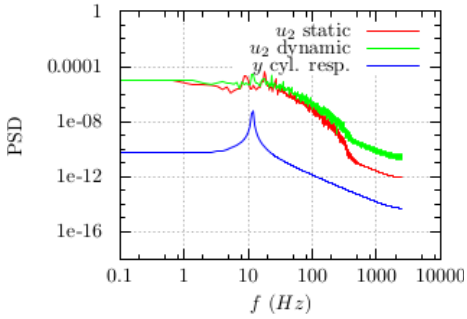

(d) Location $P3$, $u_g = 0.262\ (m/s)$

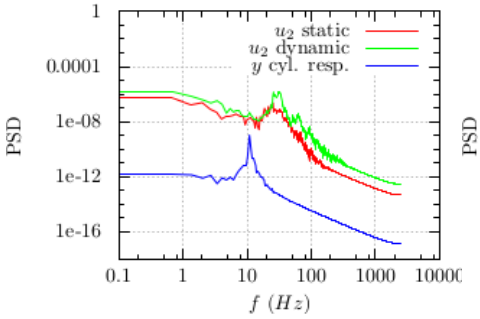

(e) Location $P1$, $u_g = 0.350\ (m/s)$

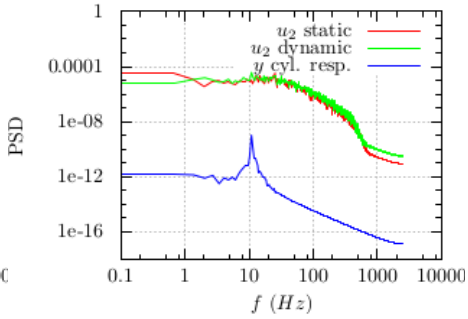

(f) Location $P3$, $u_g = 0.350\ (m/s)$

Figure 3: Power spectral densities (PSD) of Y velocity in static and dynamic cases at an upstream (P1) and a downstream (P3) locations, in comparison with the cylinder response spectrum

a distinct frequency at the cylinder response frequency ($f_n = 11.7\ Hz$). Further, the cylinder response spectrum at this velocity ($u_g = 0.262\ m/s$) is elevated in spectral power compared to the response spectra at both $u_g = 0.175\ m/s$ and $u_g = 0.35\ m/s$ gap velocities, indicating a possibility of the synchronisation between the shear layer

frequencies and cylinder response frequency. The flow velocity spectra at gap velocity $u_g = 0.35\ m/s$ show a wider peak at frequency $22.5\ Hz$, at the upstream ($P1$) location only. The frequency peak corresponding to the cylinder vibration do not reflect in the velocity spectra (Figures 3(e) and 3(f)). The shear layer frequencies increase with further increase in Reynolds number. The fluid-elastic instability in LES calculations occurs at Reynolds number $Re_g = 5310$, where the flow frequencies at upstream locations ($P1$, $P2$) are about $\sim 38.5\ Hz$ and no distinct frequency peak at downstream locations ($P3$, $P4$). In this way, the time periodicity in flow is less likely the cause of fluid-elastic instability.

The interactions between the cylinder and its adjacent flow streams can be monitored at the interface, the cylinder surface, by means of the fluid forces. The pressure force constitutes major part of the fluid force, even at these low Reynolds numbers ($Re_g \approx 6000$). The time evolution of pressure profiles on cylinder surface in static and dynamic configurations is presented in Figure (4). The time duration considered on y axis is $0.2\ s$, which approximately corresponds to two periods of the cylinder frequency in water ($f_n \approx 11.5\ Hz$). In all static case configurations (Figures 4(a), 4(c), 4(e) and 4(g)), the pressure profiles evolve symmetrically in time with respect to the azimuthal angle $\theta = 180^o$. The pressure profile in static case at intertube velocity $u_g = 0.175\ m/s$ (Figure 4(a)), when compared with the dynamic case (figure 4(b)) at same intertube velocity shows more or less symmetrical time evolution with $\sim 40\%$ increase in the pressure drop in dynamic case. The time-pressure profiles in static and dynamic cases at gap velocity $u_g = 0.262\ m/s$ are compared in Figures 4(c) and 4(d) respectively. It shows a considerable difference in the time-evolution and the value of pressure drop. The pressure difference in dynamic case has increased by ~ 3 times the static case. The pressure time evolution is changed from symmetrical to nearly antisymmetric with respect to $\theta = 180^o$ location. It indicates that, one flow stream adjacent to the cylinder ($\theta = 0^o$ to $\theta = 180^o$) when exerts positive pressure on the cylinder, the other flow stream ($\theta = 180^o$ to $\theta = 360^o$) exerts negative pressure on the cylinder surface. Further increase in intertube velocity to $u_g = 0.35\ m/s$, results in a symmetry of the time-evolving pressure profile in dynamic case, similar to the static case for the same Reynolds number (Figures 4(f) and 4(f) respectively). The value of instantaneous pressure drop is $\sim 14\%$ higher in dynamic case. The cylinder oscillations become unstable at intertube velocity $u_g = 0.437\ m/s$. The transient development of the pressure profile in dynamic case is shown in Figure 4(h). The pressure profile is antisymmetric with sudden increase in pressure drop value (to $1000\ Pa$) against the symmetrical pressure profile in static case (Figure 4(g)) with pressure drop of $220\ Pa$. The dynamic interaction between the cylinder and adjacent flow streams results in changing the time-pressure profile on cylinder surface for increasing intertube velocity (Figures 4(b), 4(d), 4(f) and 4(h)).

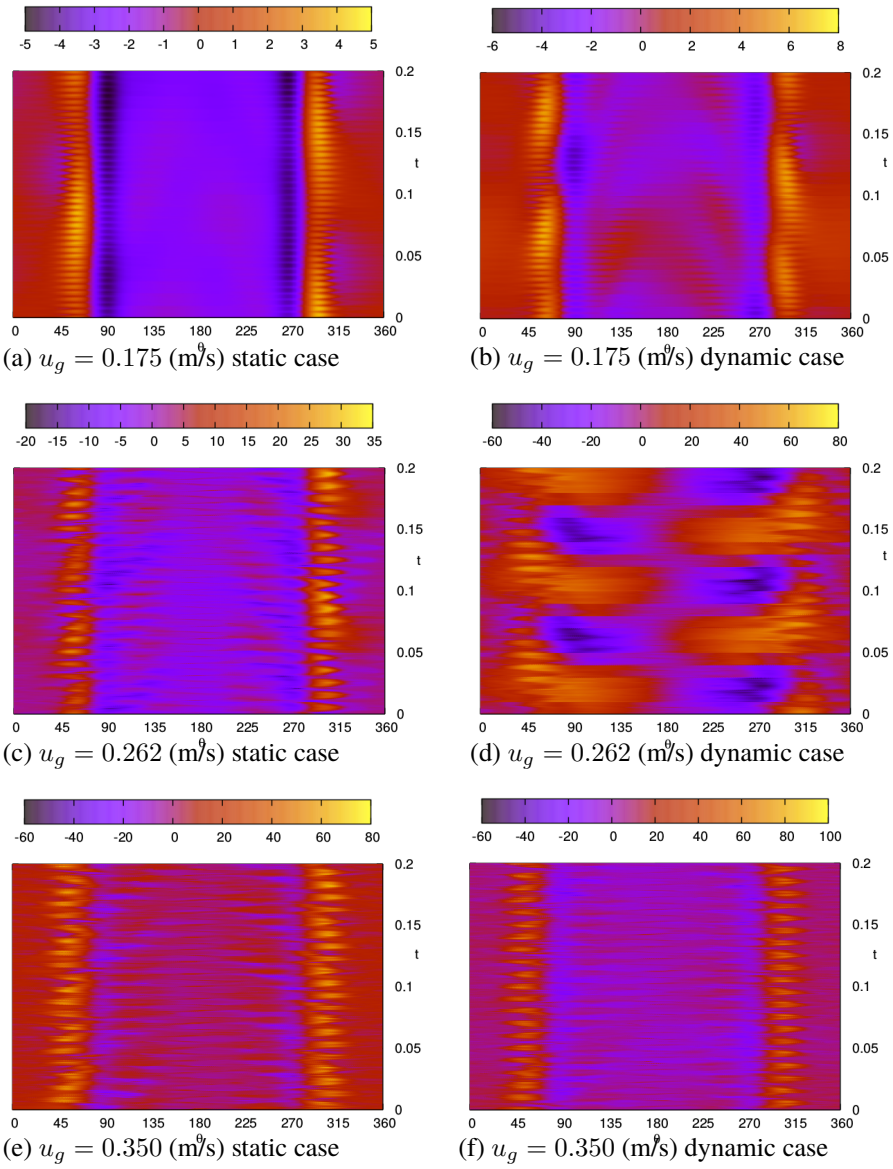

(a) $u_g = 0.175$ (m/s) static case

(b) $u_g = 0.175$ (m/s) dynamic case

(c) $u_g = 0.262$ (m/s) static case

(d) $u_g = 0.262$ (m/s) dynamic case

(e) $u_g = 0.350$ (m/s) static case

(f) $u_g = 0.350$ (m/s) dynamic case

Figure 4: Comparison of time evolving instantaneous surface pressure between static and dynamic cases

4 Conclusion

Large Eddy Simulation (LES) carried out to study fluid structure interaction in an in-line cylinder array. An Arbitrary-Lagrangian-Eulerian (ALE) approach is adapted to

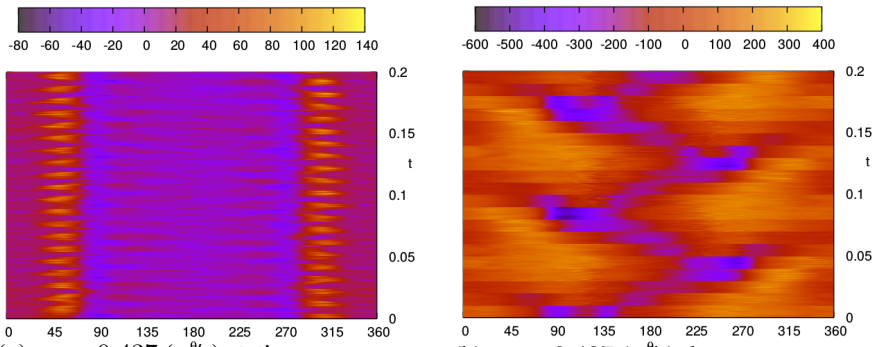

(g) $u_g = 0.437$ (m/s) static case (h) $u_g = 0.437$ (m/s) dynamic case

Figure 4: Comparison of time evolving instantaneous surface pressure between static and dynamic cases

simulate the coupling of fluid flow and motion of cylinder. The response frequency (f_n) and damping ratio (ζ) of the cylinder for the range of reduced velocities are in agreement with the experimental values. This shows, the dynamic unsteady interactions between fluid load and cylinder vibration are well captured by LES. In the analysis, we shed some light on the dynamic interactions of the cylinder vibration and the adjacent flow streams. The time evolution of the pressure profiles on the cylinder surface is indeed linked with flow stream perturbations induced by the cylinder vibration.

Acknowledgement

The authors acknowledge Centre National de la Recherche Scientifique (CNRS) for facilitating the work via Agence Nationale de la Recherche (ANR) project Baresafe.

References

[1] A. Khalifa et al., 2012. A single flexible tube in a rigid array as a model for fluidelastic instability in tube bundles. J. of Fluids and Structures 34, 14-32.

[2] A. Khalifa et al., 2013. Modeling of the phase lag causing fluidelastic instability in a parallel triangular tube array. J. of Fluids and Structures 43, 371-384.

[3] B. Anderson et al. 2014. Modeling of fluidelastic instability in a square inline tube array including the boundary layer effect. J. of Fluids and Structures 48, 362-375.

[4] B. W. Roberts, 1966. Low frequency aeroelastic vibrations in a cascade of circular cylinders. Mechanical Engineering Science No. 4.

[5] Blevins, R., 1974. Fluid-elastic whirling of a tube row. J. of Pressure Vessel Tech. 96, 263-267.

[6] C. Liang, G. Papadakis 2007. Large eddy simulation of cross-flow through a staggered tube bundle at subcritical Reynolds number. J. of Fluids and Structures 23, 1215-1230.

[7] Connors H.J., 1970. Flow induced vibration of Heat Exchanges, pp 42-56. New York:ASME Fluidelastic vibrations of tube arrays excited by cross flow.

[8] Granger, S., and M. P. Paidoussis. An improvement to the quasi-steady model with application to cross-flow-induced vibration of tube arrays. Journal of Fluid Mechanics 320 (1996): 163-184.

[9] H. Tanaka, S. Takahara, 1981. Fluid elastic vibration of tube array in cross flow. J. of Sound and Vibration 77(1), 19-37.

[10] J. H. Lever, D. S. Weaver, 1982. A theoretical model for fluid-elastic instability in heat exchanger tube bundles. J. of Pressure Vessel Tech. 104, 147-158.

[11] Jus Y., Longatte E., Chassaing J.-C., et al., 2014. Low Mass-Damping Vortex-Induced Vibrations of a Single Cylinder at Moderate Reynolds Number J. Pressure Vessel Technol. 136(5), 051305.

[12] Longatte, E. et al., 2013. Advanced numerical methods for uncertainty reduction on prediction of heat exchanger dynamic stability limits : review and perpectives. Nuclear Engineering and Design 258, 164-175.

[13] Paidoussis, M. P., Price, S. J., 1988. The mechanisms underlying flow-induced instabilities of cylinder arrays in crossflow. J. of Fluid Mechanics 187, 45-59.

[14] N. K.-R. Kevlahan, 2011. The role of vortex wake dynalics in the flow-induced vibration of tube arrays. J. of Fluids and Structures 27, 829-837.

[15] P. Rollet-Miet et al. 1999. LES and RANS of turbulent flow in tube bundles. Int. J. Heat and Fluid Flow 20, 241-254.

[16] Price, S. J., 1995. A review of theoretical models for fluid-elastic instability of cylinder arrays in cross-flow. J. of Fluids and Structures 9, 463-518.

[17] S. Benhamadouche, D. Laurence, 2003. LES, coarse LES, and transient RANS comparisons on the flow across a tube bundle. Int. J. Heat and Fluid Flow 24, 470-479.

[18] S. J. Price and M. P. Paidoussis, 1989. The flow-induced response of a single flexible cylinder in an in-line array of rigid cylinders. J. of Fluids and Structures 3, 61-82.

[19] S.S. Chen, 1983a. Instability mechanisms and stability criteria of a group of circular cylinders subjected to cross flow. I. Theory. J. of Vibration, Acoustics, Stress and Reliability in Design 105, 51-58.

[20] S.S. Chen, 1983b. Instability mechanisms and stability criteria of a group of circular cylinders subjected to cross flow. II. Numerical results and discussion. J. of Vibration, Acoustics, Stress and Reliability in Design 105, 253-260

[21] S. S. Paul et al., 2008. Experimental and numerical investigation of turbulent cross-flow in a staggered tube bundle. Int. J. Heat and Fluid Flow 29,387-414.

[22] V. Shinde et al. 2014. Numerical simulation of the fluid structure interaction in a tube array under cross flow at moderate and high Reynolds number. Journal of Fluids and Structures 47, 99-113.

[23] Y. A. Hassan, H. R. Barsamian 2004. Tube bundle flows with the large eddy simulation technique in curvilinear coordinates. International Journal of Heat and Mass Transfer 47, 3057-3071.

[24] H. R. Barsamian, Y. A. Hassan 1997. Large eddy simulation of turbulent crossflow in tube bundles. Nuclear Engineering and Design 172, 103-122.

[25] Weaver, D., 2008. Some thoughts on the elusive mechanism of fluid elastic instability in heat exchanger tube arrays. flow-induced vibration. In: The 9th international conference on flow-induced vibration. Prague, Czech Republic.